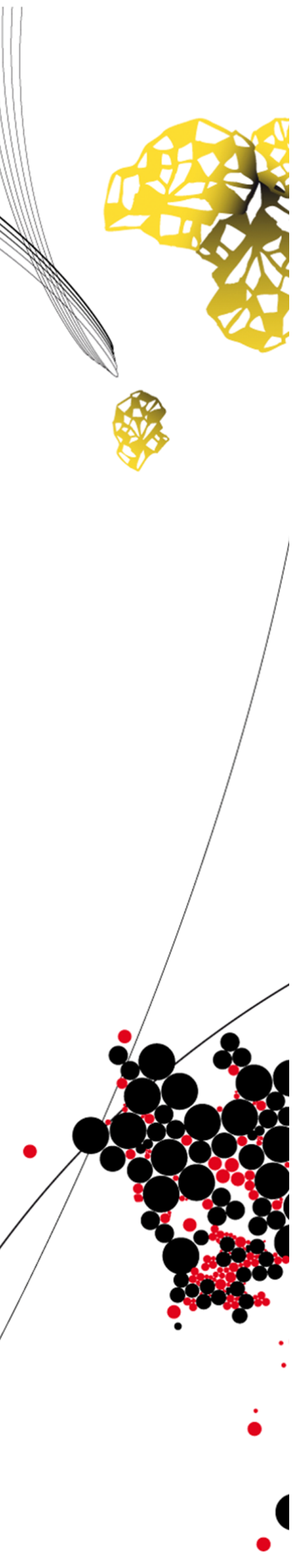

UNIVERSITY OF TWENTE.

Faculty of Electrical Engineering, Mathematics & Computer Science

Modeling and Characterizing a Sun Sensor for Nano Satellites

K.J.C. den Hollander s1478915

B.Sc. Thesis

February 2017

Supervisors:
Dr. ir. M.J. Bentum
Dr. ir. G.L.E. Monna
M.Sc. P.K.A. van Vugt

Telecommunication Engineering Group
Faculty of Electrical Engineering,
Mathematics and Computer Science
University of Twente
P.O. Box 217
7500 AE Enschede
The Netherlands

Hyperion Technologies B.V.
Motorenweg 5M
2623 CR Delft
The Netherlands

Summary

Nanosatellites require small components such that all the necessary instruments and hardware fit into the satellite. The company Hyperion Technologies have developed an Sun sensor for this application. The benefit of this Sun sensor is that it is small and relative cheap.

The Sun sensor determines the attitude of the sensor with respect to the Sun and consists of a quadrature photodiode that outputs four currents. Over the sensor a mask with a square hole is placed. The output of the four photodiodes depends on the angles between the sensor and the Sun. From this information a Sun vector is derived.

In this report the sensor is modeled, characterized and calibrated to give the sensor an accuracy of approximately 1 degree or better.

The Sun sensor provides information for the attitude determination and control system. The attitude determination system uses the information of different sensors and combines this information to determine the attitude of the satellite.

A model of the output currents of the sensor has been developed, which is used to determine the theoretical accuracy. A sensor has been measured for calibration, and a fine mesh of datapoints is measured in the experiment to calibrate the sensor numerically due to the nonlinear behavior of the sensor. From this measurements is has been seen that the calibration of the sensor is almost impossible due to the nonlinear behavior of the signal.

The conclusions are that the sensor has not been calibrated to the desired accuracy of 1 degree. The model that has been developed describes variables with the most influence on the accuracy of the sensor.

Recommendations are given to improve the sensor and achieve a better response of the signal.

Preface

This thesis has been written for my bachelor assignment of the study Electrical Engineering at the University of Twente in Enschede. For my thesis I wanted to contribute to the TwenteSat project, which is a student project at the University of Twente that wants to build a satellite for OLFAR. This is a mission that wants to measure low frequency radio waves in space. My initial plan was to build an attitude determination system, but this turned out to be too ambitious. My mentor Mark Bentum brought me in contact with Hyperion Technologies who had the assignment to work on their Sun sensor. During this assignment I gained a lot of knowledge about Sun sensors, attitude determination systems and satellites.

I would like to thank Bert Monna and Steven Engelen for their help during my bachelor assignment and Mark Bentum for his help and providing the contact with Hyperion Technologies.

Contents

Chapter 1

Introduction

1.1 Context

With the current trend of devices that are getting smaller and use less power, satellites are also shrinking and come available in areas that can benefit from this trend. For example the CubeSat [1], a standardized nanosatellite that can be designed by scientists, companies or universities [2] [3] in order to have a mission with a small payload. These satellites can have different payloads, from transponders to cameras or research instruments.

All these satellites need a system that determines their attitude with respect to an object in space, for example the Earth. This attitude determination system uses different attitude sensors that are based on different principles. One of these principles is determining the attitude with respect to the Sun. A Sun sensor determines a Sun vector and can be used in the attitude determination system. A Sun vector discribes the attitude of the Sun with respect to the sensors coordinate system. The company Hyperion Technologies B.V. has developed a Sun sensor that works with four photo diodes to determine the Sun vector. These four photo diodes are illuminated depending on the attitude between the Sun and the sensor and from this information the Sun vector can be derived.

In general, two types of Sun sensors are available, coarse Sun sensors and fine or digital Sun sensors [4]. Coarse or analog Sun sensors consist of photodiodes or solar cells that generate a current that depends on the attitude between the Sun and the sensor. Digital Sun sensors usually have an array of photodiodes. An example are CCD-cameras that determine the Sun vector. The benefit of digital Sun sensors is that they are more accurate but also have a small field of view [4]. Coarse Sun sensors have a more wide field of view but are less accurate because the same signal is spread over a larger field of view. The advantage of the coarse sensor that will be tested in this report is that it has a very small package and is relative cheap.

On commercial satellites, coarse Sun sensors are often used to bring the Sun in the field of view of the fine Sun sensor, or aim the solar panels to the Sun.

Advantages of a Sun sensor is that the Sun is very clear present in space. A clear distinction from other light illuminating or reflecting bodies in space can be made easily, for example the reflections of the Sun from the Earth or the Moon. The disadvantage is that the sensor will only work when it is illuminated by the Sun. When the satellite is in an Low-Earth-Orbit and is behind the Earth no Sun vector can be derived. This means that for approximately half of the time the sensor will not see the Sun, depending on the orbit. For satellites that have another type of orbit this could be different. The shape of the CubeSat satellite makes it necessary to use 6 Sun sensors to cover the complete area around the satellite.

1.2 Objectives

The goal of this report is to model, characterize and calibrate the Sun sensor that has been designed by Hyperion Technologies B.V. The desired accuracy of the Sun sensor is approximately 1 degree or better.

1.3 Report structure

In Chapter 2 the mechanical, electrical and software properties are described, together with general properties about the use and implementation of the sensor in a satellite.

In Chapter 3 the model of the sensor will be described. An overview will be given of the effect of the Sun on the sensor and the currents that are expected from the sensor. The theoretical accuracy of the sensor is described. A qualitative description is given about other light sources that has influence on the accuracy and the temperature influence.

In Chapter 4 the characterization is described. Here the influences of the different deviations in the sensor are given.

In Chapter 5 the sensor calibration is described. The measurements are performed on the sensor and the deviations are determined. As last an calibration curve is derived on the measured errors in the signal.

In Chapter 6 and 7 the conclusion and recommendations are given.

Chapter 2

The Sun sensor

2.1 General properties

The Sun sensor is a device that can determine the attitude between the sensors coordinate system and the Sun the so-called Sun vector. This information is used by the attitude determination system of the satellite. This system often works together with an attitude control system that can give the satellite the desired attitude. Such an attitude determination system uses multiple sensors for accuracy and redundancy. This can be star trackers, Earth sensors, magnetic field sensors or Sun sensors. The output of all these sensors are combined by the attitude determination and control system (ADCS) to control the satellite.

An advantage of this Sun sensors is that it is small and cheap. This is due to the simple electronics that can be used because the analog signal that is given by the sensor is relative strong. One side of the PCB holds the photo diode sensor with the custom mask and a thermistor for measuring the temperature of the mask, this can be seen in Figure 2.1. The other side is fitted with all the hardware for measuring and interpretation of the signals, this can be seen in Figure 2.2.

To show the working principle, an example is shown in Figure 2.3 and 2.4. When there is zero degree angle between the sensor and the Sun, both of the illuminated areas are the same. When there is an angle between the sensor and the Sunlight a larger area is illuminated on one photodoide and a smaller area is illuminated on the other photodiode. This change in illuminated area can be seen in the measurements of the current.

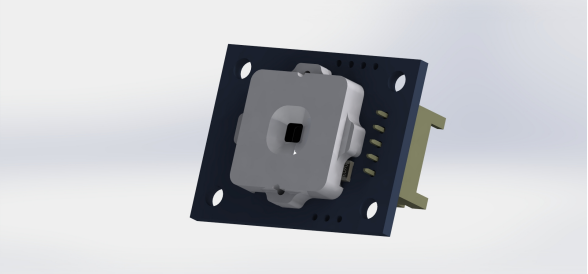

Figure 2.1: Impression of the front side of the sensor with the quadrature photodiode

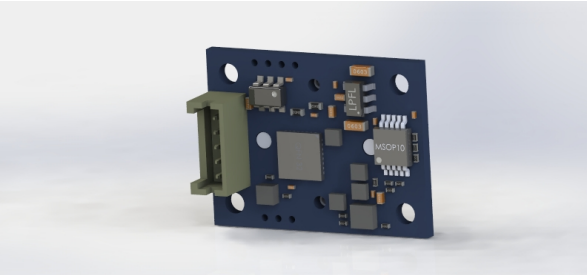

Figure 2.2: Impression of the back side of the sensor with the electronic hardware

2.2 Mechanical properties

The PCB that hold all the components is 15 by 20 mm and has a height of approximately 6 mm without the connector.

The field of view of the sensor depends on the design of the mask. The mask has a square hole with lengths of 1.64 mm. The chamfer around the hole is $120°$. This makes the sensor suitable for a field of view of approximatly $90°$. The field of view is the total angle that is observable by the sensor. When the sensor is used in a Cubesat the field of view must be greater than $90°$ to have overlap of the field of views of different sensors. This is necessary to cover the complete area around the satellite. With the design of the mask it is assumed that the sensor has a field of view of $100°$. An example of the overlapping field of views can be seen in Figure 2.5.

The sensor should operate in the harsh environment of space. The components that are used are selected by their working temperature such that they can handle this environment. Space environment can cause the temperature of the components to be from -130 to 100 degree Celcius [5]. A high radiation is also present in space. This can ,for example, distord the electronics in the satellite or the sensor. In commercial satellites radiation hardened electrical components are used to be less sensitive to this radiation. A CubeSat has usually a limited mission time of a few months. For this lifespan it is not necessary to use these expensive hardened components. Therefore on this sensor, components are used that have a large tem-

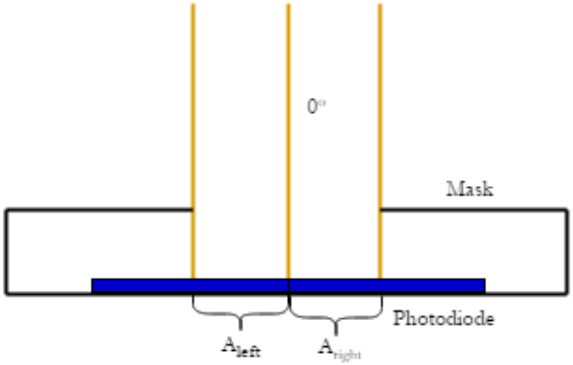

Figure 2.3: Example of the working principle with 0 degree angle

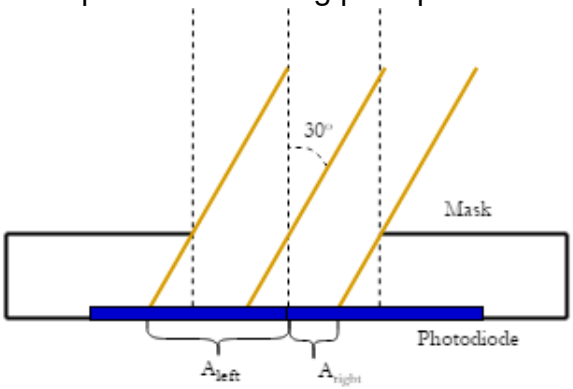

Figure 2.4: Example of the working principle with a 30 degree angle

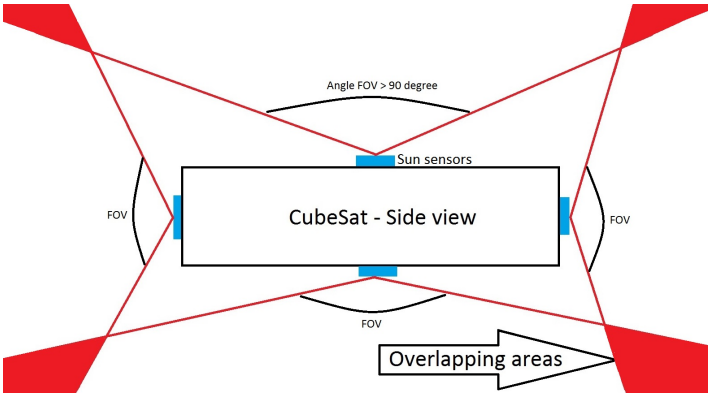

Figure 2.5: Example of overlapping field of views of a CubeSat

perature range and are very small such that the probability of being hit by radiation is small.

2.3 Electrical properties

The sensor is connected to the attitude determination and control system. Communication is done via an I2C bus. The sensors are slave devices and the attitude computer asks for the Sun vector from each sensor. The supply voltage of the sensor is provided via the same connector as the communication bus.

The electrical circuit measures the four currents of the photodiodes and the signal from the thermistor one by one. The circuit consist of an op-amp and FET's for selecting the photodiodes and connect it to the analog-to-digital converter(ADC). The op-amp makes a transimpedance amplifier to convert the current to a voltage that can be measured. A simplified diagram of the readout electronics is shown in Figure 2.6.

The sensor that is used has 4 photodiodes which have a common cathode. This means that current is going into the sensor from the measuring circuit. This makes the signal inverted, a maximum ADC value is no current from the photodiode and a minimum ADC value means that the signal to the ADC is clipping to the COMMON level.

The COMMON level in Figure 2.6 is present to raise the lower limit of the ADC because the lower range of the supply voltage holds unwanted non-linearities such as ground bounce which can distord the reading of the ADC.

When a measurement of a photodiode is taken the FET that connects the photodiode to COMMON is closed and the FET that connects the photodiode with the transimpedance amplifier is opened. Then the measurement is started and a burst of ADC conversions is executed. This is done to average the signal and reduce the influence of the noise. The transient phenomena on the measuring line are canceled by waiting a certain time after selecting the photodiode such that the transient phenomena has disappeared. When the measurement is done, the FET to the transimpedance amplifier is closed and the FET to the COMMON is opened, then using the same procedure the next photodiode is measured.

After the measurements of the photodiodes and the thermistor, an offset measurement is performed. All the FETs to the photodiodes are closed and the output of the transimpedance amplifier is measured. This is done to see if there is an offset in the transimpedance amplifier. With the measured offset, the measurements of the photodiodes can be compensated.

When all the photodiodes are measured, the Sun vector can be calculated. This is done using the algorithm that is described in Section 2.5. Also the calibration curve that will be determined is applied to the data. Now the satellite controller can pick up the Sun vector data.

The thermistor is not connected to the transimpedance amplifier but is a voltage

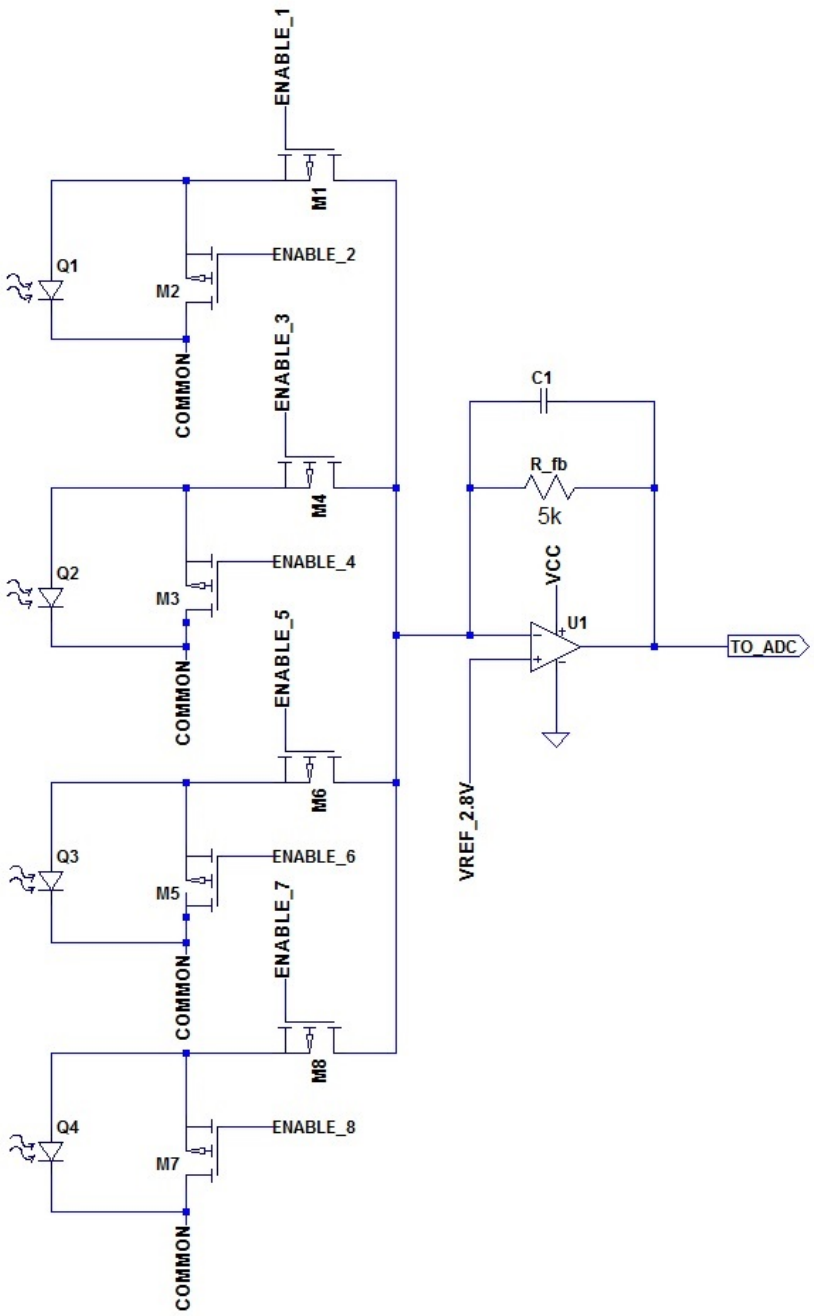

Figure 2.6: The electrical circuit of the Sun sensor

divider with another resistor and is connected to another pin on the microcontroller. This pin is internally connected to the ADC.

When the photodiode signal is measured it must be constant or slow varying to have a good determination. When a photodiode is selected by the microcontroller a transient effect will occur on the measuring line. This transient phenomena is present due to the combination of the feedback resistor $R_{feedback}$ and capacitor C_1 in Figure 2.6.

To have a sensor accuracy of 1%, the maximum deviation of the measured signal value is 1%, because the assumed field of view of the sensor is 100 degree. To be sure that the transient effect is negligible the deviation is chosen to be less than 0.1%. For the signal to reach 99.9% of the final value, a minimum of 6,9 RC-times have to be waited. The used equation can be found in Equation 2.1. Solving this equation numerically gives an RC-time of 6,9.

$$100(1 - exp^{-x}) = 99.9 \tag{2.1}$$

The gain of the feedback resistor $R_{feedback}$ is calculated by dividing the maximum input voltage to the ADC by the maximum current from the photodiode. The value of this feedback resistor is approximately 5000 Ohm.

2.4 Software properties

The software on the microcontroller controls the selection of the quadrants and thermistor, the measuring of the output signal of the op-amp and thermistor and the communication with the controller of the satellite. Also the calculations are done to calculate the Sun vector.

To handle the selection and measurement of the quadrants and the thermistor, a loop has been designed that controls the selection of the quadrants or thermistor and the start of the measurements. The complete program is interrupt driven and a timer is used to control the flow of the operations. The run time of the loop is approximately 8 milliseconds. In Figure 2.7 a simplified flowchart shows the flow of the program.

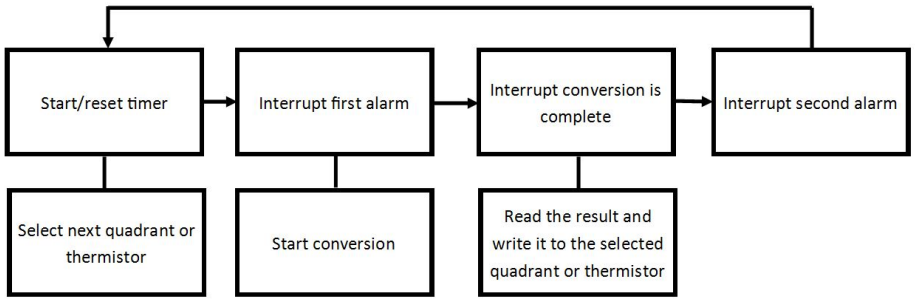

Figure 2.7: Flowchart of the microcontroller

When the timer starts, the next quadrant or thermistor is selected by controlling the output pins of the microcontroller. When the interrupt of the first alarm comes up the conversion is started. The interrupt between the selection and starting of

the conversion is present to wait for the transient effect on the measuring line to be within the desired range. After the conversion is started an interrupt will come up when the conversion is completed. Then the conversion result is read and saved. When the second interrupt comes up the next quadrant is selected and the timer is reset. The time between the first and second interrupt will give the ADC enough time to perform an ADC burst and average the results.

The calculation of the angles is done after the readout of the four quadrants and the measurement of the offset. The time between the first and second interrupt is taken long enough for the microcontroller to perform and ADC burst and calculate the angles all within the same time.

The four quadrants and the offset are measured sequentially, this is done in a few milliseconds. The measured signal is assumed to be constant. This is done because the rotational speed of the satellite, with exception after deployment, is very slow. It is assumed that the satellite will only rotate at frequencies below 1-2 Hz, the signal will therefore also be within this frequency range. Therefore when one measurement is done within a few milliseconds the signal can be assumed constant.

The communication with the satellite controller is interrupt driven and is done between the execution of the scheduled tasks.

2.5 Sun vector determination

The equation that is used to determine the angle in the x-direction can be found in Equation 2.2 and 2.3 [6] and can be used to determine the angle in the y-direction.

$$\frac{tan(\phi)}{tan(\phi_{max})} = \frac{(I_1 + I_2) - (I_3 + I_4)}{I_1 + I_2 + I_3 + I_4} \tag{2.2}$$

$$\frac{tan(\theta)}{tan(\theta_{max})} = \frac{(I_1 + I_4) - (I_2 + I_3)}{I_1 + I_2 + I_3 + I_4} \tag{2.3}$$

When the two angles are calculated they are compensated with the calibration curve that will be determined in Chapter 5.

The signals are measured in Volt. The signals are prepared to be used in the calculations with the measurement of the offset and are converted into currents using the value of the feedback resistor $R_{feedback}$. This can be seen in Equation 2.4.

$$I_i = \frac{U_i - U_{offset}}{R_{feedback}} \text{ for } i \in 1, .., 4 \tag{2.4}$$

The definitions that are used can be seen in Figure 2.8.

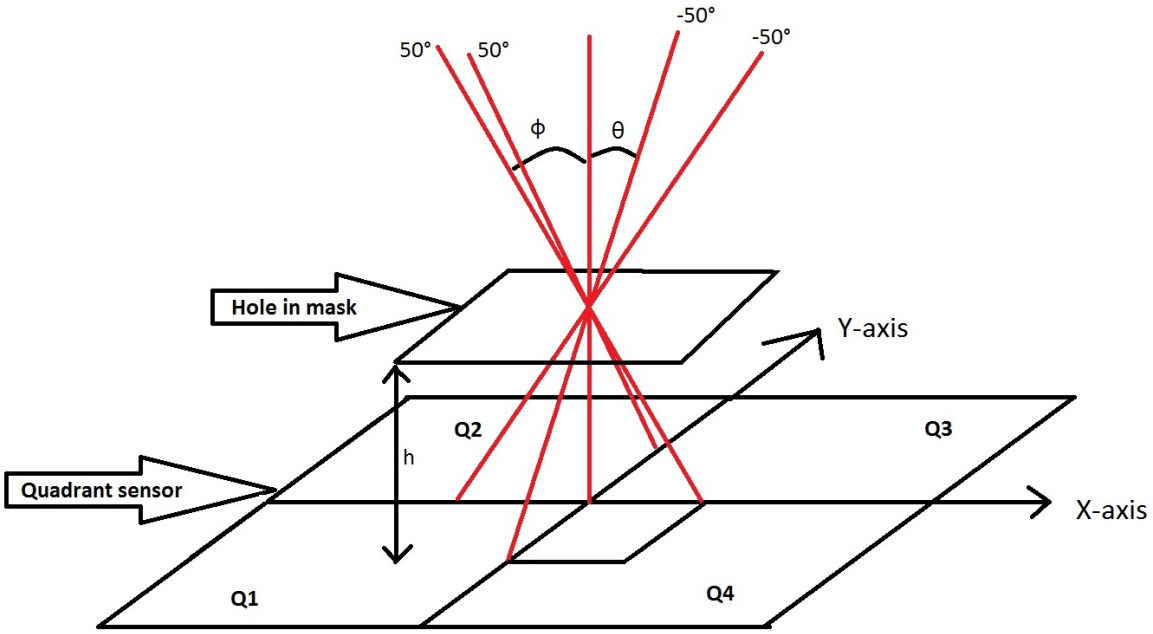

Figure 2.8: The used definitions in the determination of the angles

Chapter 3

Model of the sensor

In this section the model of the Sun sensor is described. First an equivalent circuit has been developed to show which variables are present. These variables are modeled and are used to model the accuracy of the readout electronics.

3.1 Equivalent circuit of the photodiode

An equivalent circuit has been developed that identifies all the signals and noise contributions inside the photodiode. The equivalent circuit can be seen in Figure 3.1.

The most left part in the circuit represents the photodiode, this component works together with the current source I_P. This dependent current source I_P represents the linear relation between the light power and the responsivity of the diode. This responsivity has a minimum value of 0.45 mA/mW [7]. This current source is the desired signal of the photodiode.

The I_{sp} source generates the shot noise due to the photo diode current. Shot noise is present due to the statistical fluctuations of the mechanism that controls the current of the photodiode [8].

The I_t source generates the thermal noise. Thermal noise is present due to

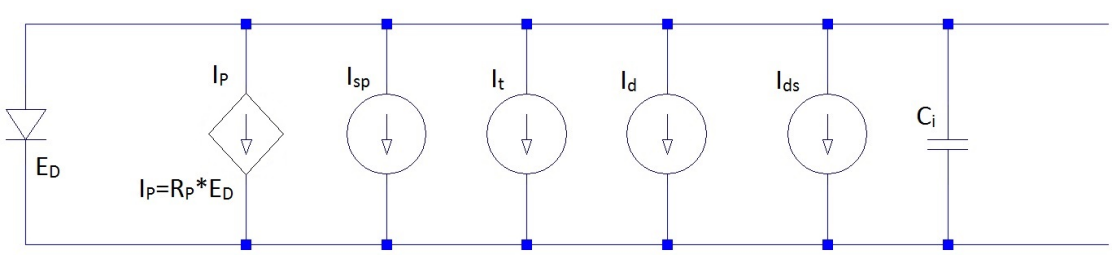

Figure 3.1: Equivalent circuit model of a single photodiode

the random movement of the electrons which is thermally induced [8]. If the feedback resistor $R_{feedback}$ would be at a temperature of zero Kelvin, there would be no movement and thus no thermal noise.

The I_d source generates the dark current. Dark current is present due to the statistical fluctuations in the photodiode when no light is received [8]. The value of the dark current is 30 nA [7].

The I_{ds} source generate the shot noise due to the dark current. These are the statistical fluctuations in the mechanism that generates dark current [8].

The capacitance C_i in the circuit represents the capacitance of the photodiode. The value of the capacitor is 10 pF [7]. This capacitance has an influence on the time constant of the of the signal I_P.

The quantization noise will also be modeled in the noise current. This noise is not present in the equivalent circuit. But is generated in the analog-to-digital converter when the signal is sampled at a finite amount of sampling levels.

3.2 Signal current

The current source I_P in the equivalent circuit is modeled here. The current that is generated has a linear relation with the area of a single photodiode that is illuminated. Also the intensity of the Sun and the responsivity are linear related to the current. In Equation 3.1 the relation between these variables is given. I_P represents the signal current, A_P represents the illuminated area, E_P represents the intensity from the Sun and R_P represents the responsivity of the photodiode.

$$I_P[A] = A_P[m^2]E_P[\frac{W}{m^2}]R_P[\frac{A}{W}] \tag{3.1}$$

The Sunlight intensity on the sensor depends on the angle between the Sun and the sensor, this relation is given in Equation 3.2. Where E_s is the intensity of the sun, which is 1367 W/m^2 [5]. The angle ϕ represents the angle in the x-direction and the angle θ represents the angle in the y-direction. Figure 3.2 shows the received intensity from the Sun that illuminates the sensor.

$$E_m = cos(\theta)cos(\phi)E_S \tag{3.2}$$

The intensity of the Sun on the sensor is symmetric around the zero degree axis. But this is not true for the current that is generated by the diode. Because the area that is illuminated will become smaller on one side of the photodiode if the angle becomes smaller and the illuminated area will become larger if the angle becomes larger. The equations for the illuminated areas are given in Equation 3.5 to 3.8. These equations are derived from Figure 3.3, this is a top view of the sensor. In

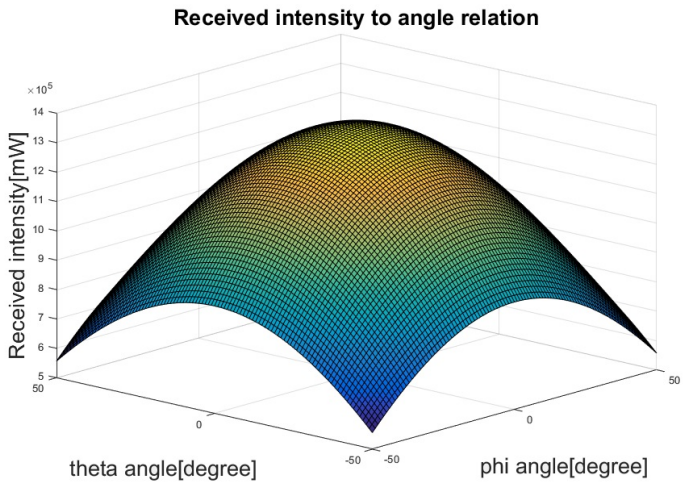

Figure 3.2: Light intensity that falls on the sensor

Appendix A is the complete derivation of the areas. When the sensor is assembled this is not done perfectly. There are tolerances between the mask and the sensor and this leads to misalignment of the sensor and the mask. This misalignment represents itself in a combination of a rotation and translation of the mask over the sensor. In this model a perfect sensor is assumed with no rotation and translation.

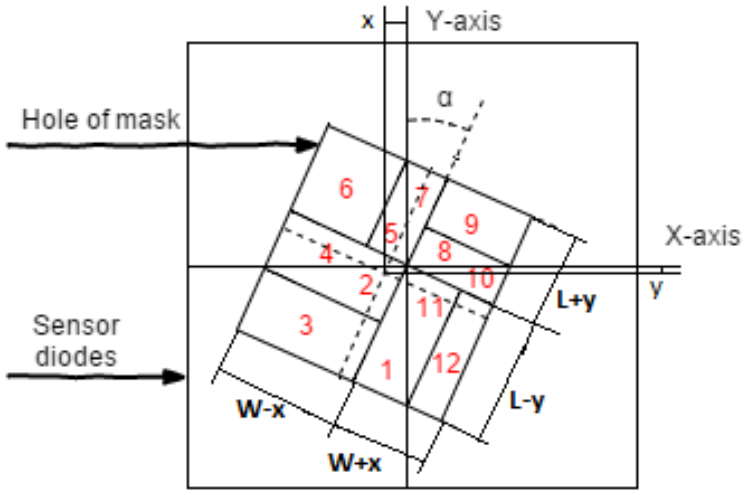

Figure 3.3: Scheme used for the derivations of the equations for the area

The values Δx and Δy represents the extra area that is illuminated due to an angle between the Sun and the sensor. These values are derived from Figure 3.4 and are defined in Equation 3.3 and 3.4, this is done in a two-dimensional figure due to symmetry of the sensor. The $cos(\alpha)$ is present in this equation due to the rotation

that can be present of the mask over the sensor.

$$\Delta x = tan(\phi)cos(\alpha)H_m \tag{3.3}$$

$$\Delta y = tan(\theta)cos(\alpha)H_m \tag{3.4}$$

In the equations W represents half the length of the total width of the hole of the mask, L represents half the length of the total length of the hole of the mask, x represents the translation of the mask in the x-direction and y represents the translation of the mask in the y-direction. The angle α represents the rotation of the mask over the sensor.

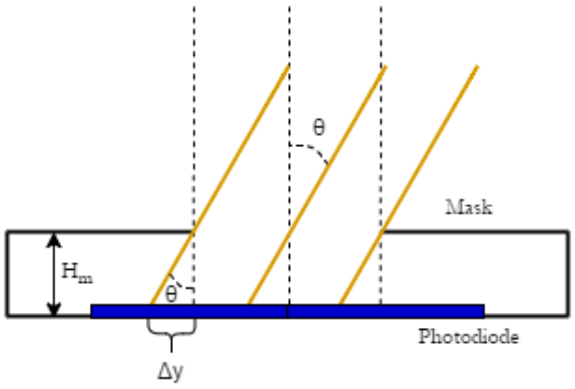

Figure 3.4: Scheme used for the derivations of the equations for Δx and Δy

$$A_1 = -\frac{1}{2}tan(\alpha)(L-y-\Delta y)^2+\frac{1}{2}tan(\alpha)(W-x-\Delta x)^2+(L-y-\Delta y)(W-x-\Delta x) \tag{3.5}$$

$$A_2 = -\frac{1}{2}tan(\alpha)(W-x-\Delta x)^2+\frac{1}{2}tan(\alpha)(L+y+\Delta y)^2+(W-x-\Delta x)(L+y+\Delta y) \tag{3.6}$$

$$A_3 = -\frac{1}{2}tan(\alpha)(L+y+\Delta y)^2+\frac{1}{2}tan(\alpha)(W+x+\Delta x)^2+(W+x+\Delta x)(L+y+\Delta y) \tag{3.7}$$

$$A_4 = -\frac{1}{2}tan(\alpha)(W+x+\Delta x)^2+\frac{1}{2}tan(\alpha)(L-y-\Delta y)^2+(W+x+\Delta x)(L-y-\Delta y) \tag{3.8}$$

Now when all the variables are known the functions can be plotted, this can be seen in Figure 3.5. When the Sun comes from exactly above, the angle ϕ and θ are zero and all the diodes give the same output current. When for example the

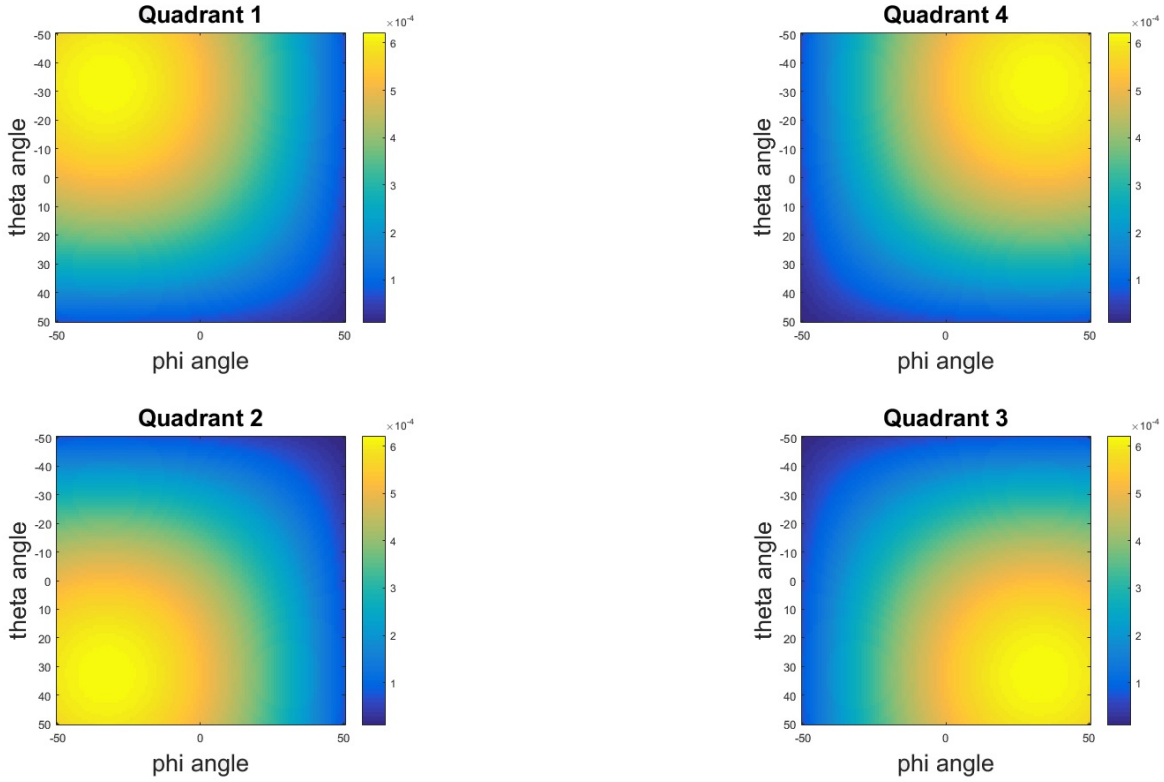

Figure 3.5: Current out of the photo diodes

angle for only ϕ becomes larger the current from the left two diodes of the sensor will become lower and the two right diodes will give a higher output current.

The maximum current out of the diodes is approximately 0.6 mA, the minimal current of the diodes is approximately 9.6 uA. This value can be used in the determination of the effective number of bits of the ADC and the determination of the theoretical accuracy.

The divergence of the light and the thickness of the mask are neglected in this model because their maximum influence is only 0.41%. This value is assumed negligible.

3.3 Noise current

In this section the noise current is modeled and is later used to determine the theoretical accuracy of the readout electronics.

3.3.1 Thermal noise

Thermal noise current can be calculated using Equation 3.9 [8]. Thermal noise comes from the feedback resistor of the transimpedance amplifier.

$$I_t^2 = \frac{2kTB_n}{R_{feedback}} \tag{3.9}$$

The value of the thermal noise is $3.75 * 10^{-22}A$. Assuming a temperature of 470 Kelvin, a feedback resistor of 5 Kilo Ohm and a bandwidth of 318 Hz.

3.3.2 Shot noise

The shot noise consists of two parts, shot noise due to the current that is generated by the photodiode and shot noise due to the dark current. These values are describe in Equation 3.10 and 3.11 [8]. The value of the dark current I_d is 30 nA [7].

$$I_{sp}^2 = 2qB_nI_P \tag{3.10}$$

$$I_{ds}^2 = 2qBI_d \tag{3.11}$$

The maximum value of the shot noise due to the photodiode current is $5.32 * 10^{-23}A$ and the shot noise due to the dark current is $3.05 * 10^{-24}A$. Assuming a bandwidth of 318 Hz.

3.3.3 Quantization noise

The value of the quantization noise can be calculated using Equation 3.12. The amount of used bits by the ADC is 12.

$$I_Q^2 = \frac{1}{12}(\frac{LSB}{R_{feedback}})^2 \tag{3.12}$$

The current due to quantization noise is $1.79 * 10^{-15}A$ assuming a feedback resistor of 5 Kilo Ohm.

3.4 Estimation of the accuracy

When all the values of the noise and signal strengths are known, an estimation of the accuracy can be made. The maximum total noise current is $3 * 10^{-8}A$. The

minimal signal current is $9.6 * 10^{-6}A$.

$$ENOB = \frac{{}_{10}log\frac{I_{signal}}{I_{noise}}}{{}_{10}log(2)} \tag{3.13}$$

The effective number of bits can be calculated using Equation 3.13. The effective number of bits is minimal 8.32 bits. This means that there are 320 effective levels. To have an accuracy of 1 degree over a field of view of 100 degree this means that 100 effective levels are necessary. Therefore the accuracy reached by the readout electronics is high enough to reach an sensor accuracy of 1 degree. The accuracy of the readout electronics is calculated in Equation 3.14 and is $0.31°$.

$$Accuracy = \frac{FOV}{2^{ENOB}} \tag{3.14}$$

3.5 Reflections inside mask

When the diodes are illuminated part of this light is reflected back on the mask. Because the mask is parallel with the sensor, the mask will reflect back onto the diode and more current will be generated. The mask is colored black and will therefore have less reflection than the diode itself.

It is assumed that the current that is generated by the reflections of the mask is smaller than 1 LSB and will therefore not be noticable in the measured signal.

3.6 Albedo model

When the sensors are in space, reflections of the Sun from the Earth will disturb the received light. This light will disturb the signal and the sensor will calculate a distorded Sun vector.

An Albedo model can be added in the controller of the sensor that compensates for these reflections. But for this the reflections must be known under different attitudes, positions of the satellite and the configuration of the Earth, Sun and satellite.

Albedo models are available [9] that approximate the reflections of the Earth. With the Sun sensor it is possible to make a model. The Sun sensor measures in fact the power of light that falls on the sensor and can thus be used as an powermeter. When this data is collected at a lot of places it can be used to make a model and calibrate the sensor using this model.

3.7 Temperature influence on sensor

The maximum and minimum temperature of the sensor lie within the range of -130 to 100 degree Celcius [5]. This large range has influence on the expension of the mask and the responsivity of the photodiodes.

When the mask is heated it will expand. If this expension happens uniformly the change of the size of the hole is predictable. But in space the Sun only comes from one direction and the heating of the mask will only be at one side if the angle between the Sun and the sensor is large. The heating of the sensor will be quite rapid due to the abscence of an atmosphere. Therefore this heating will be very local. When there is no uniform heating the shape of the square hole can change and this could have a large effect on the calculation of the angle.

The responsivity of the photodiodes will also dependent on the temperature. This has an influence on the calculation of the Sun vector. When this change in responsivity is modeled the calibration curve can compensate this effect.

Chapter 4

Sensor characterization

The characterization of the sensor is the determination of what influence a certain deviation can have with respect to an ideal sensor. An overview is given of the different simulated deviations and their effects on the calculation of the angles ϕ and θ.

4.1 Ideal sensor

When the sensor is build and no misalignments are present, the output angles that are calculated do not have an error. In the x-direction where the angle ϕ is calculated the values of the angles in the y-direction are constant. In the y-direction where the angle θ is calculated the values of the angles in the x-direction are constant. Because the sensor is perfectly build the angle ϕ and θ do not have an effect on each other. The currents and output angles are shown in Figure 4.1.

4.2 Effect of responsivity deviation

According to the datasheet of the quadrant photodiode the minimal responsivity is 0.45 mA/mW. Because it is a minimum value the responsivity of the four quadrants can be different and this has an effect on the output currents and the calculated output angles. A plot has been made for a sensor with different values of the responsivity for every quadrant. This can be seen in Figure 4.2.

When the angle between the Sun and the sensor changes the output currents will all change at a different rate because of the different responsivities. It can be seen in the two most right subplots of Figure 4.2 that this happens on a slow rate and a clean curve without sudden changes. Therefore this change in responsivities should be calibratable with a polynomial function.

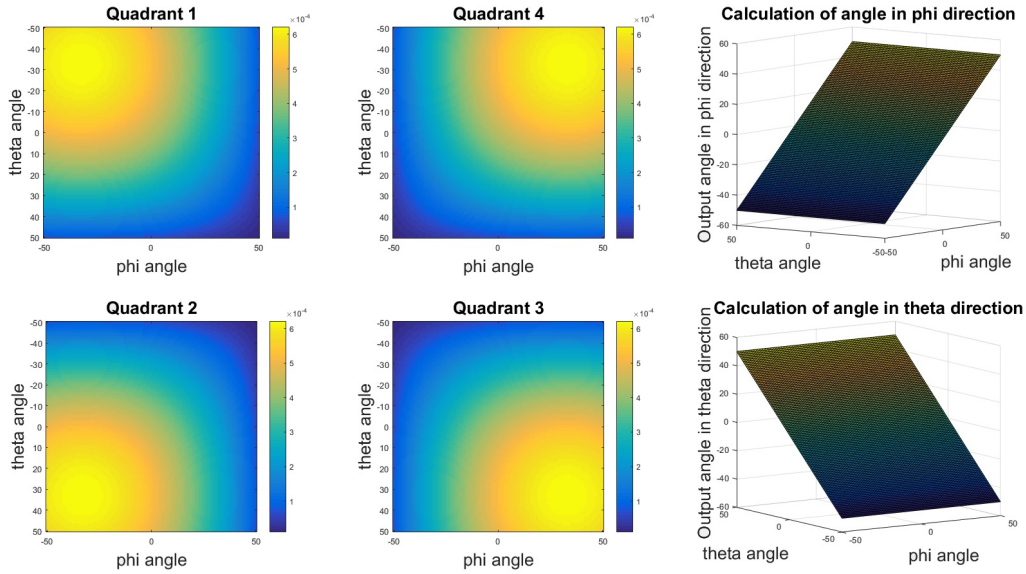

Figure 4.1: Output currents and angles of an ideal sensor

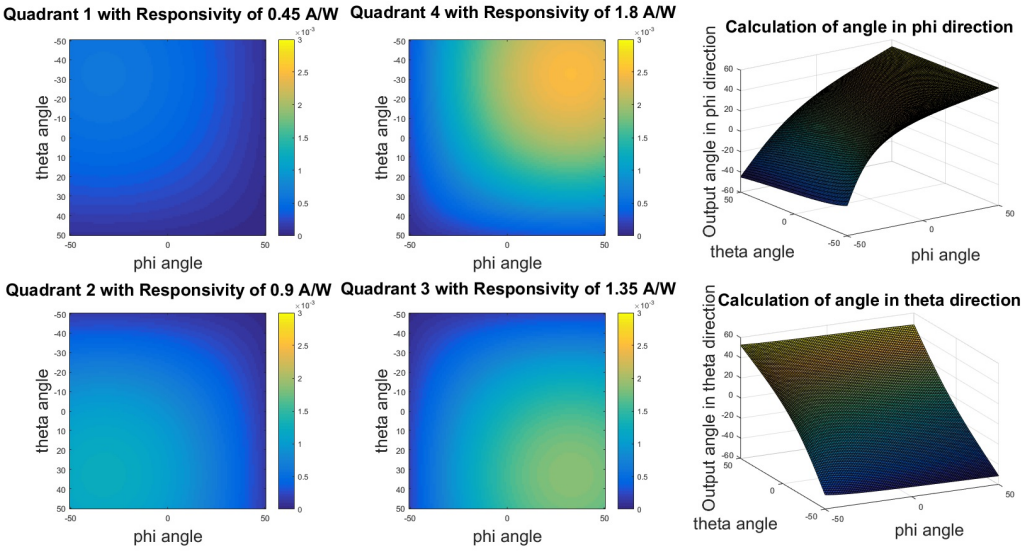

Figure 4.2: Output currents and angles for a sensor with different responsivities

4.3 Effect of translated mask

When a translation is present of the mask over the sensor, some photodiodes will receive more light than the other photodiodes. This translation has an effect on the calculations of the angle. A plot has been made for a translation in the x-direction of 0.5 mm and can be seen in Figure 4.3. This translation has the same effect in the y-direction. Only in that case the translation has an effect on the calculation of the

angle θ.

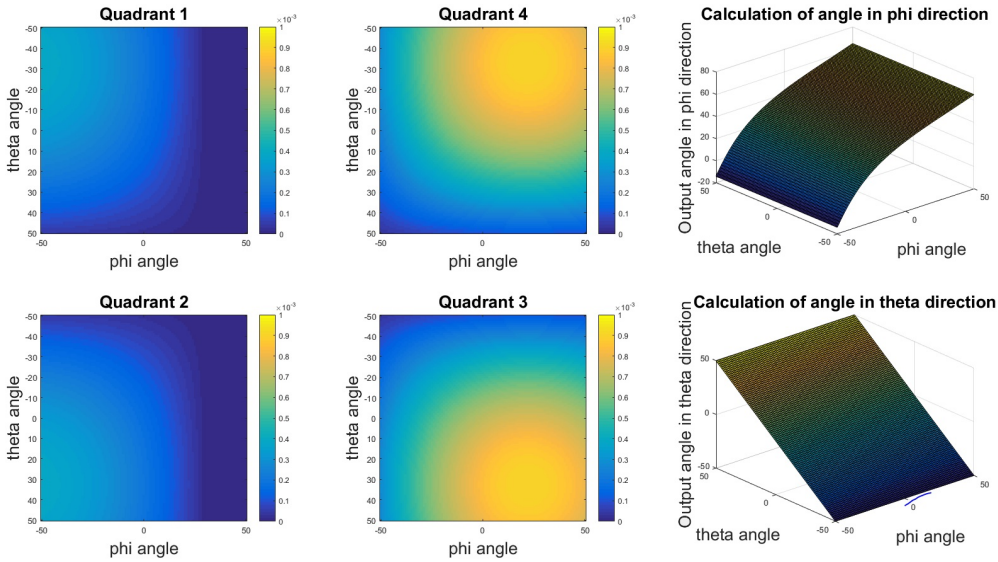

Figure 4.3: Output currents and angles for a sensor with a translated mask in the x-direction

The change of the angle ϕ have another ratio in the currents due to the translation and are therefore not a clean inverse tangent line. But instead a shifted and scaled version of it. This curve changes at a slow rate and with no sudden changes and should therefore be calibratable with an polynomial function.

4.4 Effect of rotated mask

The mask can be rotated over the sensor. When there is a rotation, the combination of angles where the highest currents occure are rotated too. This has an influence in the calculation of the angles and can be seen in Figure 4.4.

From the simulation it can be seen that the calculated angles have a smooth change from the ideal output. This should be calibratable using a polynomial function.

4.5 Relation between rotation and translation

The mask has a maximum rotation over the sensor. This maximum angle between the sensor and the mask is 2.67 degree. When this maximum rotation is present there is no translation present because the sensor will center itself inside the square hole of the mask, assumed the hole in the mask and the sensor are perfectly square.

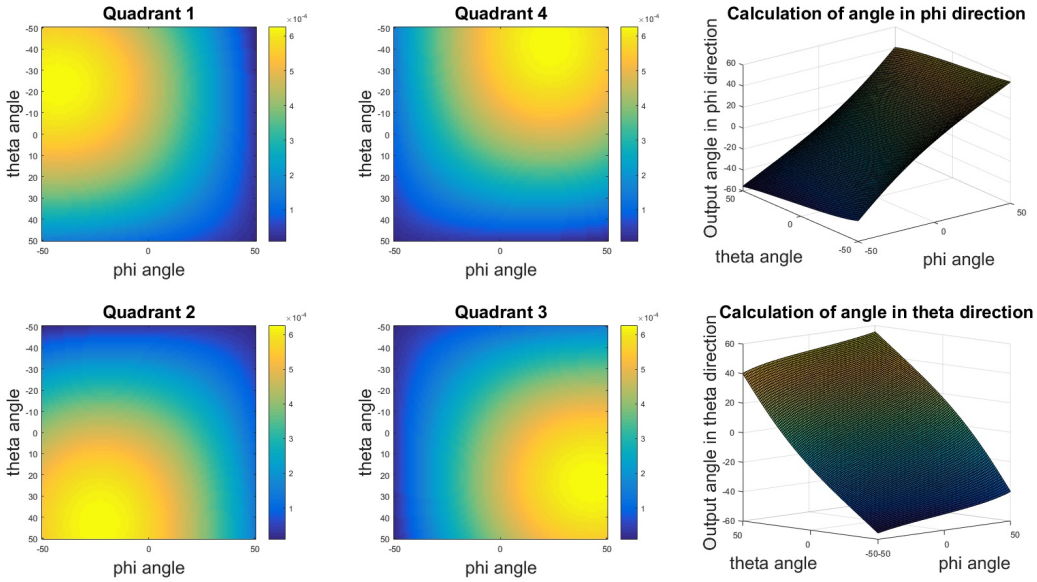

Figure 4.4: Output currents and angles for a sensor with a rotated mask of $15°$

When there is a smaller angle present between the sensor and the mask there is space left which allows the mask to have a translation.

The relation between the maximum translation that can be present and the angle between the sensor and the mask is given in Figure 4.5.

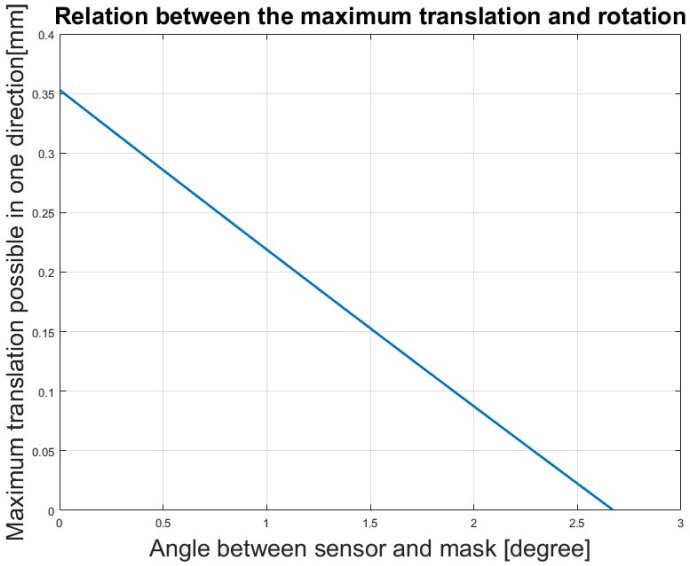

Figure 4.5: Relation between rotation of the mask to possible maximum translation

4.6 Effect of height deviation

The distance between the mask and the sensor has an influence on the accuracy of the sensor. When the mask is at a larger distance from the sensor the angles that have the highest currents are shifted outwards. This can be seen in Figure 4.6.

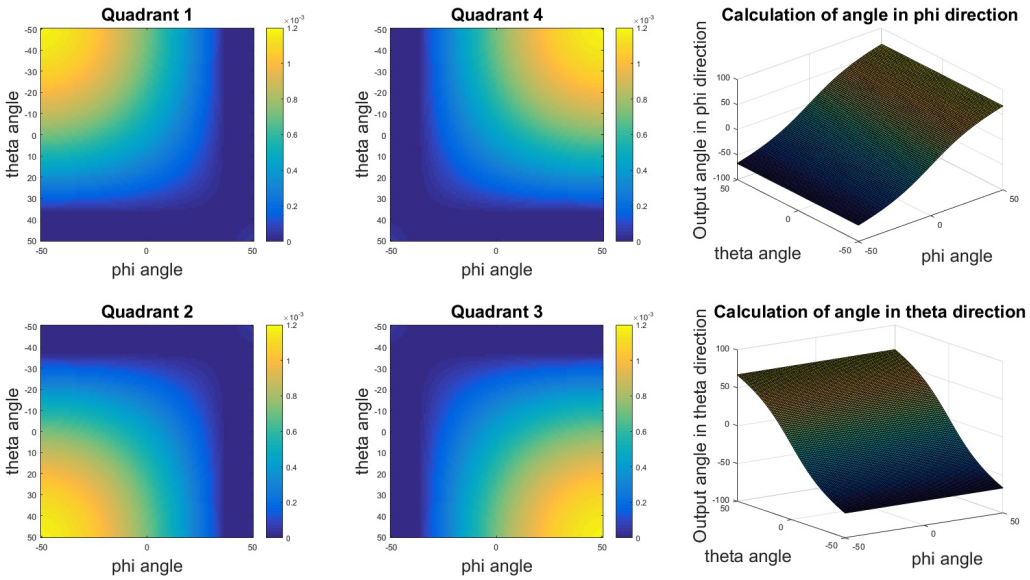

Figure 4.6: Output currents and angles for a sensor with a double height

When the angle between the Sun and the sensor changes the currents will increase more rapidly then when the mask would be closer to the sensor. Because the extra area that is illuminated, Δx and Δy, dependent on the distance between the sensor and the mask. In this way the rate of change of the illuminated areas can be controlled by changing the distance between the sensor and the mask.

4.7 Squareness of the mask

The squareness of the mask has an influence on the currents that are generated by the sensor. During the manufacturing process this must be done as precise as possible. Especially the sides of the square hole in the mask needs to be perpendicular to each other to make the hole in the mask a perfect square. This squareness also depends on the stresses in the mask due to different temperatures.

Chapter 5

Sensor Calibration

In this chapter the calibration of the sensor is described. First the measurement setup is shown and the experiment is described. Second the results of the measurements are shown and analysed. Last the calibration curve is determined and analysed.

5.1 Measurement setup

A measurement setup has been build that can rotate the sensor over two axes to the light source. The accuracy of the rotating table is approximately 1 degree. The controller of the rotating table receives the measured currents from the sensor after a new point has been reached. These are send to the computer and are saved. The measurement setup is shown in Figure 5.1.

One measurement takes approximately 1 second. When a finer mesh is used the time increases quadratically with every extra measuring point along one axis.

The rotating table has been designed such that the eye of the sensor is in the axis of rotation of both the rotating axes. In this way the light source only has to be small. If the eye would not be in the center of rotation a large beam would be needed because the eye would not only rotate but also would have a translation. This translation is canceled by placing the sensor in the rotation centers.

As a light source a laser is used. The advantage of a laser is that it has a almost perfect parallel beam and can be pointed easily on the eye of the sensor. The disadvantage is that the beam is coherent and that the power is not uniformly distributed over the beam. The beam has an elliptic shape and the power has a gaussian distribution over the height and the width of the beam.

Because the beam is not completely paralell, the size of the lightspot on the sensor increases if the laser and sensor have a larger distance. The laser is placed such that the flat top of the gaussian curve is over the eye of the sensor and that

there is no great influence of the gaussian distribution of the power.

The chamber where the experiment takes place is dark, this is done to limit the influence of the environmental light that could distort the measurements.

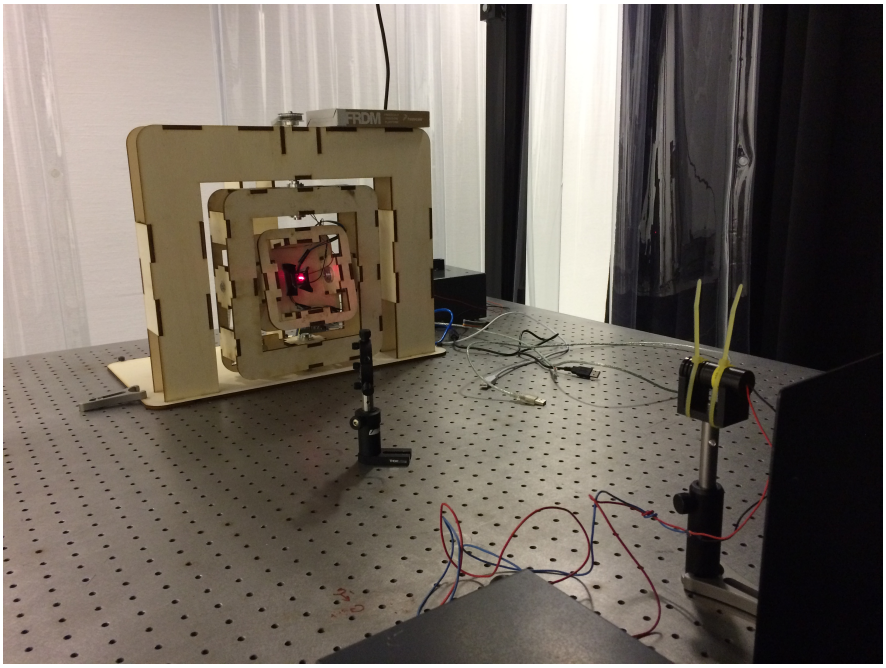

Figure 5.1: Measurement setup for determining the sensors response under different angles

5.2 Results

For this experiment a stepsize of 2 degree have been chosen. This gives an overview that is very accurate and almost measures all the points that the sensor should be able to distinguish. The results of the measurements are shown in Figure 5.2.

Analyzing the measurements it can be seen that there is a large area in every photodiode current that has a measured value of zero current, the dark blue areas. Another area that can be clearly seen is the point where the highest currents are measured, the yellow areas. In these yellow areas the voltage clips to the ADC reference.

Inbetween the areas is a very steep change in current, the current changes from zero to the maximum value in approximately 25 degree in both directions. This steep change makes the ratios that are used to determine the output angles change in a very steep rate too. Then the angle calculation is not as expected, as can be seen in the two most right subplots of Figure 5.2.

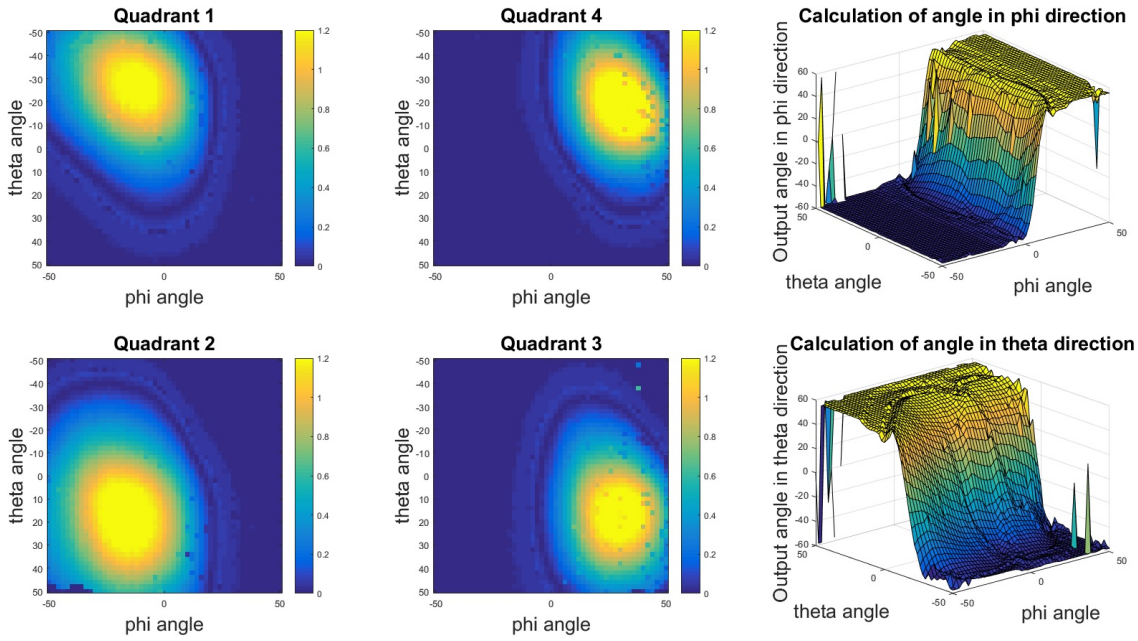

Figure 5.2: Measured data from the sensor

A hypothesis for this steep change could be attributed to the nonlinear behavior of a photodiode. Until now it is assumed that the responsivity of the photodiode has a constant value. But it can be possible that this is not the case. When enough power goes into the diode, the photodiode will start generating current. This happens at a certain amount of illuminated area. From this point on the generated current will change very fast from that point on if more area is illuminated due to a change in angle between the sensor and the light source.

Another hypothesis is that the area that will be extra illuminated due to an angle between the sensor and the light source changes very fast. In that case the current that is generated also changes on a fast rate. This fast rate of change in illuminated area is due to the distance between the sensor and the mask. In Equation 3.3 and 3.4 the dependency of the extra illuminated area and the distance between the sensor and the mask can be seen.

If the used light source for the experiment would have been more intense, the dark blue area would have been smaller and the yellow spot would have been larger. The reverse holds for when a beam with less intensity would have been used. The blue area would have been larger and the yellow area would have been smaller. This is because the same areas are still illuminated, only the intensity is changed. This would have no effect on the rapidly changing current and would only shift the transistion from low to high current.

Also a ring of higher values is present in the dark blue areas. These lighter

rings comes from measurement values that holds lower currents then the offset measurement. These values are filtered out and shown in Figure 5.3. From these values it can be seen that the output current first drop before they increase to the maximum value.

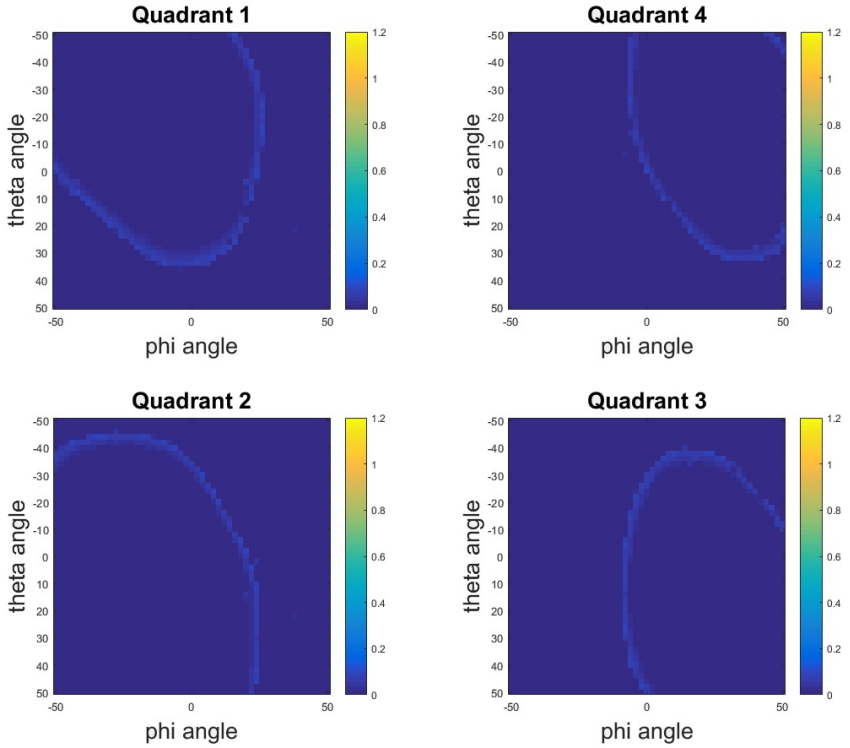

Figure 5.3: Lower than offset measurements

5.3 Determination of the calibration curve

Because the equations for determining the currents are nonlinear it cannot be solved symbolically. Therefore the calibration curve is determined numerically from the measured data.

Using Equation 5.1 and 5.2 the error of the sensor is determined. Figure 5.4 are the errors that are used to determine the calibration curve.

$$\phi_{error} = \phi_{ideal} - \hat{\phi} \tag{5.1}$$

$$\theta_{error} = \theta_{ideal} - \hat{\theta} \tag{5.2}$$

Using the curve fitting tool from MATLAB a polynomial has been derived that fits the datapoints from Figure 5.4. The dots are the datapoints from Figure 5.4, the

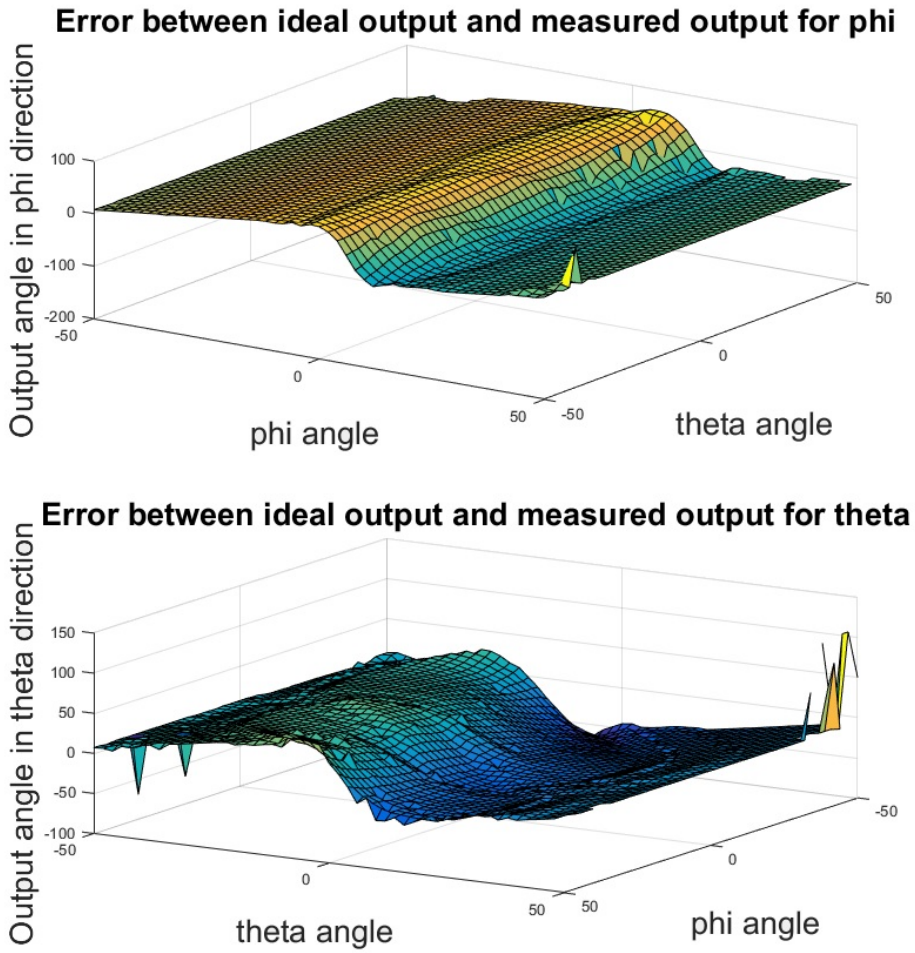

Figure 5.4: Errors between the desired ideal output and the measured data

surface is the fitted polynomial. The fitted curve for angle ϕ can be seen in Figure 5.5 and the fitted curve for angle θ van be seen in Figure 5.6.

Analyzing this calibration curve it is seen that there is a very large deviation between the calibration curve and the error. A 5th order polynomial has been used but this is not able to follow the steep changes in the error. The residual for the curve fit for ϕ angle ranges from almost zero to more then 30 degree. The residual for θ angle ranges from almost zero to more than 20 degree. It can be seen that this polynomial is not able to achieve the desired accuracy.

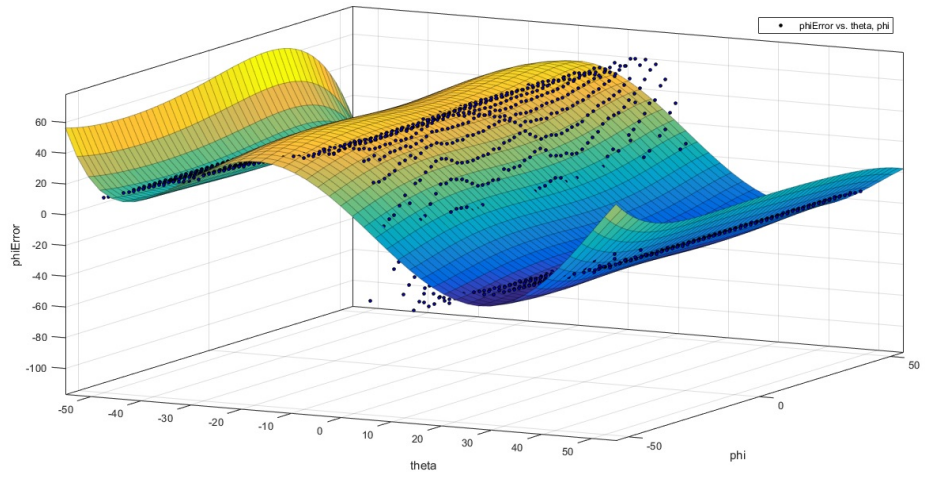

Figure 5.5: Calibration curve for the phi angle

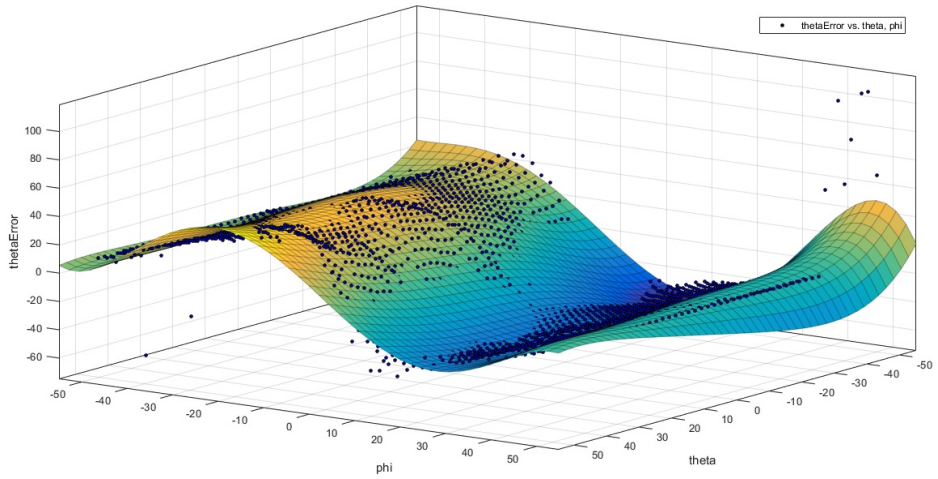

Figure 5.6: Calibration curve for the theta angle

Chapter 6

Conclusion

The desired accuracy of the sensor is 1 degree. According to the measurements and calibration this accuracy has not been reached with the calibration of the sensor.

The model that has been developed describes the variables that have the most influence on the accuracy of the sensor. These are the translation in the x and y-direction, the rotation of the mask and the height between the sensor and the mask. The output currents from the four photodiodes can be simulated using this model.

The sensor is calibrated numerically due to the nonlinear model of the sensor. A polynomial calibration curve is used to approximate the error. This curve gives the sensor an accuracy of approximatly 20 degree in the θ direction and a accuracy of approximatly 30 degree in the ϕ direction.

These high errors are due to the small transisiton band that is present in the measurements of the signal. This transistion band is present due to the nonlinear behavior of the photodiode or the distance between the sensor and the mask.

Chapter 7

Recommendations

7.1 Hole in the mask

The round edges of the square hole that is in the mask limits the field of view to 45 degree. In Figure 7.1 the angle θ and ϕ are both under an angle of 50 degree. It can be seen that the chamfer with the round edges blocks the light that falls into the sensor if the angles are getting larger. It is recommended to change the design of the mask to have a more wide field of view and that there are less problems with the overlap of the different field of view of the different sensors.

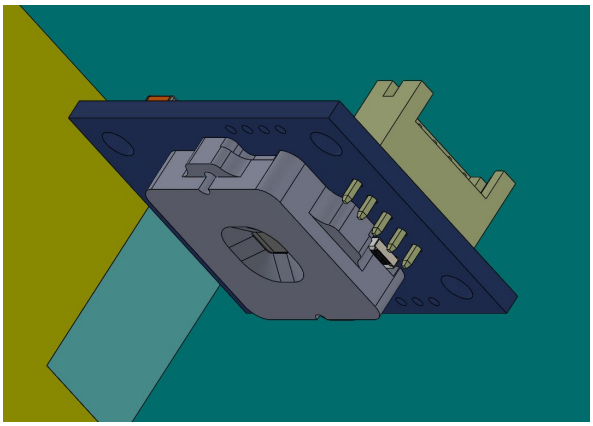

Figure 7.1: Light is blocked by the round edges of the mask

Another solution would be to limit the specified field of view on the diagonal axis. Then this problem could be solved without changing the design of the mask, this is also done by commercial Sun sensors [10].

7.2 Temperature model

A model can be added that describes the change in the dimensions of the mask dependent on the temperature. If this change is known the sensor can compensate for the non uniform expansion due to local heating and improve the accuracy of the sensor at changes in temperature.

If a temperature dependent model of the responsivity would be made, a temperature dependent calibration curve could be made and improve the accuracy of the sensor.

7.3 Nonlinear response of photodiode

The current that is generated is assumed linear in the model. But in practice this current depends on a few variables, for example the temperature of the sensor. This makes the relation between the generated current and the light power nonlinear.

This response can be added in the model together with the temperature model such that the sensor can compensate this effect and this effect has less influence on the accuracy.

7.4 Calibration curve

The calibration curve is made by using the program MATLAB is a polynomial in two directions. The weights of the points that are taken is not specified and is taken uniformly distributed over the axis. This calibration curve can be optimized if there are weights used. Some of the points that are picked by the curve fitting algorithm are not optimal. Therefore this curve fitting can be optimized such that there is less error and a higher accuracy.

For this to help the sensor must also have a more smooth transision between the maximum and minimum output value of the ADC. Such that a better fitting is possible of the calibration curve.

7.5 Dimensions of the mask

In the measurements results it has been seen that the transistion between the maximum and minimum output value of the ADC changes in approximately 25 degree. One of the hypothesis for this was that there is a too fast change in the illuminated area of the photodiodes.

The rate at which this area changes can be controlled by changing the distance between the sensor and the mask. For an optimum output current from which the angles are derived, the minimum output current should be at one side of the angles and the maximum value should be at the other side. This can be achieved by making the square hole in the mask bigger. In this way more current would be generated when there is zero angle between the sensor and the Sun. Then when this angle changes and less area would be illuminated the current would drop and when more area would be illuminated more current would be generated.

A solution would be that approximately one quarter of the maximum current would be generated if there is zero angle in both directions. In this way there is a current swing possible if there is more area illuminated and when there is less area illuminated, which is not the case in the current situation as can be seen in Figure 5.2. In this way there is also a more smooth transistion between the minimum and maximum value of the output of the ADC. Also the ratios from which the angles are derived would be more gradually changing and the error in the calculated angles would be better calibratable.

An example of this solution is shown in Figure 7.2. The red lines show the output currents and illuminated areas which allow for a greater current swing and the green lines represent the current situation. The subscripts in the areas, A, are the angles, the same holds for the currents I. The black line represents the current to illuminated area relation of the photodiode. The responsivity is assumed linear in this example.

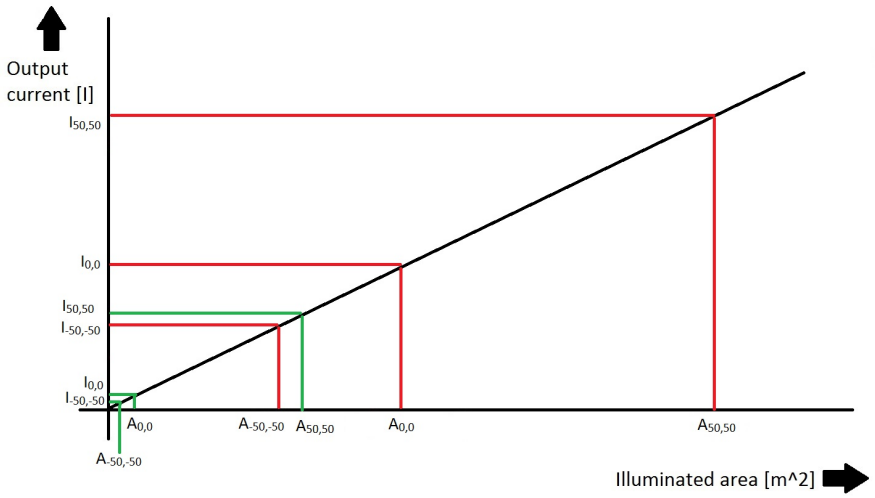

Figure 7.2: Design of the relation between output current and the illuminated area

Bibliography

[1] C. P. S. University, “Cubesat design specifications revision 12,” August 2009.

[2] M. J. Bentum, “Twentesat - the first low-frequency interferometer in space,” *63th International Astronautical Congress, Napels, Italy*, 2012.

[3] “Web site of delfi space, the tu delft small satellite program.” [Online]. Available: http://www.delfispace.nl

[4] F. L. Markley and J. L. Crassidis, *Fundamentals Of Spacecraft Attitude Determination and Control*. Springer, 2014.

[5] J. R. Wertz and W. J. Larson, *Space Mission Analysis And Design Third Edition*. Kluwer Academic Publishers, 1999.

[6] “Datasheet bison64 sun sensor,” Internal document, Lens Research and Development, December 2015.

[7] “Surface mount quad photodiode opr5911,” TT Electronics, 2015. [Online]. Available: http://www.ttelectronics.com/sites/default/files/download-files/OPR5911_RevC.pdf

[8] S. Haykin and M. Moher, *Introduction to analog & digital communications*. Wiley, 2007.

[9] D. Bhanderi and T. Bak, “Modeling earth albedo for satellites in earth orbit,” *Proceedings of AIAA conference on Guidance, Navigation and Control*, 2005.

[10] Lens Research and Development, 2016. [Online]. Available: https://lens-rnd.com/?page_id=48

Appendix A

Area derivations

Equations 3.5 to 3.8 are derived from Figure 3.3. In this appendix the complete derivation is given for the calculation of the areas.

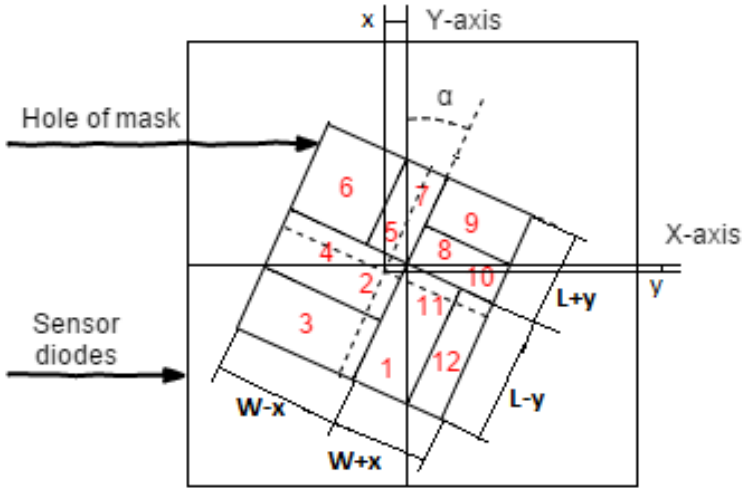

Figure A.1: Scheme used for the derivations of the equations for the area

First the equations for the illuminated areas of the different quadrants are given.

$$A_{Q1} = A_1 + A_2 + A_3 \tag{A.1}$$

$$A_{Q2} = A_4 + A_5 + A_6 \tag{A.2}$$

$$A_{Q3} = A_7 + A_8 + A_9 \tag{A.3}$$

$$A_{Q4} = A_{10} + A_{11} + A_{12} \tag{A.4}$$

Now the derivations for the numbered parts in Figure A.1 are given.

$$A_1 = \frac{1}{2}(L - y - \Delta y)^2 \tag{A.5}$$

$$A_2 = \frac{1}{2}(W - x - \Delta x)^2 \tag{A.6}$$

$$A_3 = (L - y - \Delta y)(W - x - \Delta x) - tan(\alpha)(L - y - \Delta y)^2 \tag{A.7}$$

$$A_4 = \frac{1}{2}(W - x - \Delta x)^2 \tag{A.8}$$

$$A_5 = \frac{1}{2}(L + y + \Delta y)^2 \tag{A.9}$$

$$A_6 = (W - x - \Delta x)(L + y + \Delta y) - tan(\alpha)(W - x - \Delta x)^2 \tag{A.10}$$

$$A_7 = \frac{1}{2}(L + y + \Delta y)^2 \tag{A.11}$$

$$A_8 = \frac{1}{2}(W + x + \Delta x)^2 \tag{A.12}$$

$$A_9 = (L + y + \Delta y)(W + x + \Delta x) - tan(\alpha)(L + y + \Delta y)^2 \tag{A.13}$$

$$A_{10} = \frac{1}{2}(W + x + \Delta x)^2 \tag{A.14}$$

$$A_{11} = \frac{1}{2}(L - y - \Delta y)^2 \tag{A.15}$$

$$A_{12} = (W + x + \Delta x)(L - y - \Delta y) - tan(\alpha)(W + x + \Delta x)^2 \tag{A.16}$$